Tumor Pretargeting for Radioimmunodetection and Radioimmunotherapy

Hui Zhu, Rakesh K. Jain and Laurence T. Baxter

Steele Laboratory, Department of Radiation Oncology, Massachusetts General Hospital and Harvard Medical School, Boston; and Radiological Sciences Program, Massachusetts Institute of Technology, Cambridge, Massachusetts

The limited success of the sole use of monoclonal antibodies for cancer detection and treatment has led to the development of multistep methods using antibodies in conjunction with low molecular weight agents. For tumor pretargeting, it is important to optimize dose and schedule of relevant agents and to understand barriers to targeted delivery. Here, we address these issues for the anti-carcinoembryonic antigen bifunctional antibody–hapten and the streptavidinylated antibody–biotin systems using a recently developed physiologically based pharmacokinetic model. **Methods:** For baseline conditions of a standard 70-kg man with a 20-g tumor embedded in the liver, the model was used in conjunction with the Medical Internal Radiation Dosimetry schema to: estimate absorbed doses in tumor and normal tissues; determine the dose dependence of effector agent accumulation in tumor; simulate tumor-to-background effector agent uptake ratio; and calculate the therapeutic ratio for different antibody forms and radionuclides. Alternative drug administration schemes and variable tumor physiological conditions were considered. **Results:** Model simulations showed that ^{131}I-labeled biotin with the streptavidinylated F(ab')$_2$ provided the highest therapeutic ratio under the optimized conditions. The simulations also showed that biotin with the bifunctional streptavidinylated immunoglobulin G provided the highest tumor-to-liver uptake ratio during the early period. Sensitivity analysis showed that antibody extravasation was the major factor limiting the accretion of the effector agent in tumor, whereas antigen expression in normal tissues and tumor antigen shedding had little effect on the absorbed doses. **Conclusion:** Tumor pretargeting should provide a definite advantage over direct antibody targeting with up to a 200% increase in tumor-to-background ratio in radioimmunodetection and up to a 76% increase in tumor-to-bone marrow therapeutic ratio in radioimmunotherapy. Rapid antibody clearance from the bloodstream before effector agent injection is expected to improve the therapeutic ratio marginally (3%–10%). However, continuous plasmapheresis dramatically increased the tumor-to-background ratio by a factor of 10 in RAID and the tumor-to-bone marrow therapeutic ratio by more than 110% for short-lived radionuclides in RAIT. Apart from drastic measures such as extended plasmapheresis, pretargeting selectivity was neither sensitive enough for radioimmunodetection nor effective enough for radioimmunotherapy in patients with typical solid tumors even using the optimized protocols.

Key Words: radioimmunodetection; radioimmunotherapy; tumor pretargeting; pharmacokinetic model; bifunctional antibody–hapten

J Nucl Med 1998; 39:65–76

Low tumor-to-background uptake ratio and normal tissue toxicity are the major obstacles for radioimmunodetection (RAID) and radioimmunotherapy (RAIT) with radiolabeled monoclonal antibodies (*1–9*). One strategy to overcome these obstacles is tumor pretargeting. This involves administration of a tumor targeting antibody with an extra binding site for a low molecular weight effector (imaging or therapeutic) agent, which is given (ideally) after most of the antibody has been cleared from the systemic circulation and has concentrated in the tumor (*10–19*). The low molecular weight agent clears much more rapidly from the bloodstream and sensitive normal tissues. To evaluate such complex strategies, it is essential to understand transport barriers, assess the potential of optimized clinical protocols and address limitations that remain, even under favorable conditions.

In a previous study, we addressed the optimization issues for RAID and RAIT with radiolabeled monoclonal antibodies using a physiologically based pharmacokinetic model (*20*). Using anti-carcinoembryonic antigen (CEA) murine antibody ZCE025 as an example, we concluded that RAID and RAIT with radiolabeled monoclonal antibodies alone were inadequate for cancer diagnosis and treatment; other strategies, such as tumor pretargeting, may yet be helpful in improving the modality (*20*). To evaluate the potential of these strategies, we have developed a similar physiologically based pharmacokinetic model for tumor pretargeting systems. The model is capable of describing the pharmacokinetics of an anti-CEA bifunctional antibody (BFA)–hapten system (ZCE/CHA-EOTUBE) in nude mice bearing human tumor xenografts and of predicting the pharmacokinetics of the BFA–hapten system in humans by scaling up the model parameters from mice to humans (*21*).

Here, as done previously for direct antibody targeting, we applied the pharmacokinetic model to the BFA–hapten system and the streptavidinylated antibody–biotin system to address the following critical issues in tumor pretargeting:

1. Can absorbed doses be estimated a priori from knowledge of physiological and physicochemical parameters using a mathematical model?
2. What is the proper interval between antibody injection and effector agent injection?
3. How effective is forced antibody clearance before effector agent injection?
4. What are the relationships between antibody dose, effector agent dose and effector agent uptake in tumor?
5. What are the optimal antibody and effector agent doses for a high uptake of effector agent in tumor?
6. Which antibody form, immunoglobulin G (IgG) or F(ab')$_2$, is more suitable for cancer detection?
7. What are the optimal combinations of antibody forms and radionuclides that give the highest therapeutic ratio in cancer treatment?
8. Can this strategy fulfill its promise to increase tumor-to-background uptake ratio and reduce normal tissue toxicity? and
9. How effective is tumor pretargeting under average and favorable tumor physiological conditions?

Our aim is to quantitatively assess the advantages of tumor pretargeting, comparing results with previously published studies.
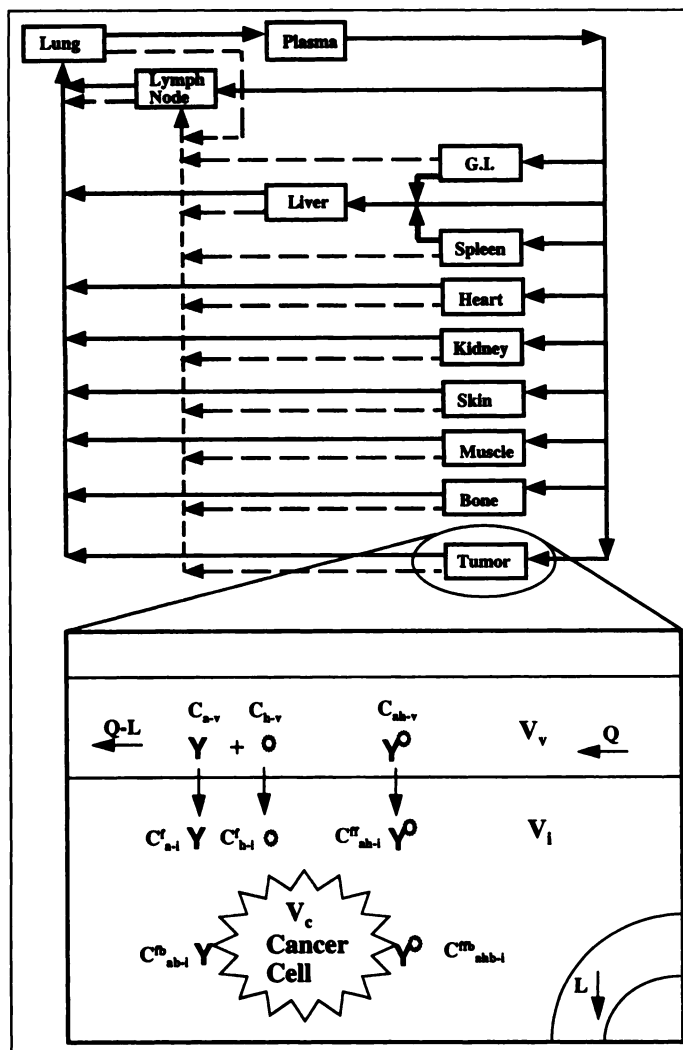
FIGURE 1. Schematic of whole-body compartments for the physiologically based pharmacokinetic model and the subcompartments for tumor. C = BFA or effector agent concentration in each subcompartment; J_{v-i} = BFA or effector agent extravasation (transcapillary exchange); $K^{f}_{antigen}$ = BFA-antigen-specific binding association rate; $K^{r}_{antigen}$ = BFA-antigen specific binding disassociation rate, L_{organ} = lymphatic flow rate; V_c, V_i and V_v = cellular, interstitial and vascular volumes, respectively; Q_{organ} = plasma flow rate.

MATERIALS AND METHODS

Physiologically Based Pharmacokinetics Model

The physiologically based pharmacokinetic model for tumor pretargeting systems was based on a previously developed phar-

macokinetic model for radiolabeled monoclonal antibodies (Fig. 1) (21). The details of model development have been presented previously (21,22). In brief, the following processes were included in the model:

1. Transport of the antibody and effector agent via the systemic circulation;
2. Extravasation (transcapillary exchange) of the antibody and effector agent;
3. Recirculation of the antibody and effector agent from the interstitial space to systemic circulation via lymphatic circulation;
4. Nonspecific binding of the antibody and effector agent in the interstitial space;
5. Specific binding of the effector agent with BFA;
6. Specific binding of the antibody and tumor antigen;
7. Catabolism of the antibody and effector agent in tissues; and
8. Renal clearance of the antibody and effector agent.

The antibody–effector agent complex was assumed to share the same transport properties and catabolism and clearance rates as the antibody itself. In the model, we chose not to include the impact of the lost labels due to the lack of experimental information and to focus on the physical properties of the radionuclides (radiation emissions and half-life). Thus, we assumed that released labels were rapidly excreted and had little impact on the observed pharmacokinetics. The model equations are given in Appendix B.

Model Parameters and Baseline Conditions

For mice, the plasma flow rates, organ volumes, antigen concentration, antibody–antigen binding kinetics, antibody–effector agent binding kinetics, the permeability–surface area products and other molecule-dependent parameters were obtained from the literature (Tables 1–3). When parameter values were not available in the literature, they were estimated with a weighted nonlinear regression fit to the experimental data of BFA-^{111}In-hapten system in mice. For streptavidinylated antibody and biotin, the transport parameters are scaled from BFA and hapten according to their molecular weights (Tables 1–3). The major difference between the two systems was the significantly higher (10^6 times) antibody–effector agent affinity between streptavidinylated antibody and biotin.

For humans, plasma flow rates and organ volumes were obtained from the literature for a 70-kg standard man (21–23). For the remaining parameters, the murine values were scaled up to humans according to known empirical relations (21,24). Vascular and interstitial volumes, together with fluid recirculation rates, were scaled up proportional to body weight. Lymphatic flow rates, permeability–surface products and urine excretion rates were scaled up from mice according to (body weight)$^{3/4}$ (21,24). Other

TABLE 1
Molecular Species-Dependent Parameters

Molecular species	σ_L	σ_S	PS$_L^{\dagger}$ (ml/min/g) Mouse	PS$_L^{\dagger}$ (ml/min/g) Human	PS$_S^{\dagger}$ (ml/min/g) Mouse	PS$_S^{\dagger}$ (ml/min/g) Human	Urine excretion rate (min^{-1}) Mouse	Urine excretion rate (min^{-1}) Human
ZCE IgG	0.26	0.98	2.66×10^{-6}	3.50×10^{-7}	7.80×10^{-6}	1.00×10^{-6}	0.00026	0.110
ZCE F(ab')$_2$	0.11	0.96	7.98×10^{-6}	1.10×10^{-6}	2.34×10^{-6}	3.10×10^{-7}	0.0011	0.446
Streptavidinylated IgG	0.26	0.98	2.21×10^{-6}	2.91×10^{-7}	6.50×10^{-6}	8.30×10^{-7}	0.00026	0.110
Streptavidinylated F(ab')$_2$	0.11	0.96	6.13×10^{-6}	8.46×10^{-7}	1.80×10^{-6}	2.38×10^{-7}	0.0011	0.446
Hapten	0.10	0.10	4.2×10^{-1}	5.5×10^{-2}	4.2×10^{-1}	5.5×10^{-2}	0.2	84.7
Biotin	0.10	0.10	3.5×10^{-1}	4.6×10^{-2}	3.5×10^{-1}	4.6×10^{-2}	0.2	84.7

*From ref. 29.
†Based on albumin data (29), scaled by diffusion coefficient in normal tissue:
$(P_1/P_2) = (MW_1/MW_2)^{-1.09}$ (33). Values for tumor and liver are assumed to be 10-fold higher than in other organs.

TABLE 2
Plasma Flow Rates and Organ Volumes*

Organ	Plasma flow rate (ml/min) Mouse	Plasma flow rate (ml/min) Human	Fluid flow rate (ml/min/g) Mouse	Fluid flow rate (ml/min/g) Human	Lymphatic flow rate (ml//min) Mouse	Lymphatic flow rate (ml//min) Human	Total volume (ml) Mouse	Total volume (ml) Human	Vascular volume (ml) Mouse	Vascular volume (ml) Human	Interstitial volume (ml) Mouse	Interstitial volume (ml) Human
Plasma	4.38	3000	N/A	N/A	N/A	N/A	0.774	2700.0	0.774	2700.0	0.000	0
Bone	0.17	138	1.4×10^{-5}	1.9×10^{-6}	6.0×10^{-5}	2.6×10^{-2}	1.500	1500.0	0.080	150.0	0.280	279.0
Heart	0.28	120	5.6×10^{-5}	7.5×10^{-6}	1.0×10^{-5}	4.3×10^{-3}	0.133	300.0	0.007	15.0	0.019	42.9
Kidney	0.80	630	5.6×10^{-4}	7.5×10^{-5}	1.7×10^{-4}	7.4×10^{-2}	0.298	284.0	0.030	28.4	0.101	96.6
Liver	1.10	800	4.6×10^{-4}	6.1×10^{-5}	2.0×10^{-4}	8.7×10^{-2}	0.951	1809.0	0.095	180.9	0.190	361.8
Lung	4.38	3000	3.0×10^{-4}	4.0×10^{-5}	1.0×10^{-4}	4.3×10^{-2}	0.191	999.0	0.019	99.9	0.057	299.7
Muscle	0.80	413	5.0×10^{-6}	6.7×10^{-7}	6.0×10^{-4}	2.6×10^{-1}	7.924	35000.0	0.150	700	1.032	4558
Skin	1.21	220	3.0×10^{-5}	4.0×10^{-6}	1.0×10^{-5}	4.3×10^{-3}	2.940	6800.0	0.200	462.0	0.999	227
Spleen	0.05	138	3.0×10^{-5}	4.0×10^{-6}	2.0×10^{-6}	8.7×10^{-4}	0.100	1734.0	0.010	17.0	0.020	34.7
Gastrointestinal tract	0.90	468	1.0×10^{-6}	1.3×10^{-7}	7.0×10^{-4}	3.0×10^{-1}	3.450	2147.0	0.100	43.0	0.600	373.2
Tumor	0.10	0.564	1.0×10^{-5}	1.3×10^{-6}	7.0×10^{-5}	3.0×10^{-2}	0.472	20.0	0.033	1.4	0.258	10.9

N/A = not applicable.
*From refs. 21 and 22.

antibody-dependent parameters such as binding kinetics, pore sizes and reflection coefficients were kept the same as in mice. These known and estimated parameters, which formed the baseline conditions in this study, are given in Tables 1–3.

Dose Calculations

Absorbed doses were calculated under the Medical Internal Radiation Dosimetry schema (23) for a hypothetical 20-g tumor embedded in the liver, as used previously (20). The following equations were used to estimate the absorbed doses in various tissues. For tumor:

$$D_{tumor} = \tilde{A}_{tumor}\Delta_{np}/M_{tumor} + (\tilde{A}_{tumor} + \tilde{A}_{n\cdot liver})\Sigma_i\Delta_i\Phi_i(\text{liver} \leftarrow \text{liver})$$
$$+ \Sigma_h\tilde{A}_hS(\text{liver} \leftarrow \text{h}).$$

For liver:

$$D_{liver} = \tilde{A}_{n\cdot liver}\Delta_{np}/M_{n\cdot liver} + (\tilde{A}_{tumor} + \tilde{A}_{n\cdot liver})\Sigma_i\Delta_i\Phi_i(\text{liver} \leftarrow \text{liver})$$
$$+ \Sigma_h\tilde{A}_hS(\text{liver} \leftarrow \text{h}).$$

For other tissues (bone marrow, heart, lung, kidney, spleen, gastrointestinal tract, skin and muscle):

$$D_{organ} = (\tilde{A}_{tumor} + \tilde{A}_{n\cdot liver})S(\text{organ} \leftarrow \text{liver}) + \Sigma_h\tilde{A}_hS(\text{organ} \leftarrow \text{h}).$$

Here, h includes bone marrow, heart, lung, kidney, spleen, gastrointestinal tract, skin and muscle; $\tilde{A}$ is the accumulated activity; Δ_i is the mean energy emitted per nuclear transition for particle i (np for nonpenetrating radiation); Φ_i (liver $\leftarrow$ liver) is the specific absorption fraction of energy for target organ liver for particle i emitted in the source organ liver; S is the mean dose per unit accumulated activity; M_{tumor} is the liver-embedding tumor tissue mass; and $M_{n\cdot liver}$ is the normal liver tissue mass (23).

Absorbed Dose Estimation

Two different pharmacokinetics were used to estimate the absorbed dose in humans for anti-CEA IgG_1 BFA–hapten system (17): empirical pharmacokinetics obtained by a curve fit and predicted pharmacokinetics from our physiologically-based model. A triexponential function, $\alpha_1exp(-\lambda_1t) + \alpha_2exp(-\lambda_2t) + (1 - \alpha_1 - \alpha_2)exp(-\lambda_3t)$, was fitted to the averaged ^{111}In-labeled hapten pharmacokinetics from 10 patients (body weight, 40–100 kg; tumor weight, 4–50 g; IgG1 BFA dose, 5–40 mg). The human data were those presented in our previous study (21). The fitted empirical pharmacokinetics were used to calculate the absorbed doses in tumor and critical normal tissues for effector agent combined with [67]Cu, ^{90}Y, ^{131}I and [188]Re. The results were compared with a priori estimates obtained using the physiologi-

TABLE 3
Parameters Fitted for Each Organ*

Organ	K^f (min^{-1}) IgG	K^f (min^{-1}) F(ab')$_2$	K^f (min^{-1}) Streptavidinylated IgG	K^f (min^{-1}) Streptavidinylated F(ab')$_2$	K^f (min^{-1}) Hapten	K^f (min^{-1}) Biotin	K^r (min^{-1}) Hapten	K^r (min^{-1}) Biotin
Bone	2.5×10^{-3}	5.5×10^{-4}	2.5×10^{-3}	5.5×10^{-4}	8.5	8.5	1	1
Heart	0.0	3.3×10^{-4}	0.0	3.3×10^{-4}	1.0×10^{-3}	1.0×10^{-3}	5.0×10^{-4}	5.0×10^{-4}
Kidney	0.0	1.2×10^{-3}	0.0	1.2×10^{-3}	2.1×10^{-2}	2.1×10^{-2}	1.0×10^{-3}	1.0×10^{-3}
Liver	0.0	3.6×10^{-4}	0.0	3.6×10^{-4}	2.0×10^{-3}	2.0×10^{-3}	7.0×10^{-4}	7.0×10^{-4}
Lung	0.0	3.0×10^{-5}	0.0	3.0×10^{-5}	4.0×10^{-3}	4.0×10^{-3}	2.0×10^{-3}	2.0×10^{-3}
Muscle	0.0	2.4×10^{-4}	0.0	2.4×10^{-4}	1.5×10^{-3}	1.5×10^{-3}	5.0×10^{-4}	5.0×10^{-4}
Skin	0.0	7.5×10^{-2}	0.0	7.5×10^{-2}	2.5×10^{-3}	2.5×10^{-3}	5.0×10^{-4}	5.0×10^{-4}
Spleen	0.0	6.5×10^{-2}	0.0	6.5×10^{-2}	3.0×10^{-4}	3.0×10^{-4}	5.0×10^{-5}	5.0×10^{-5}
Gastrointestinal tract	0.0	7.5×10^{-4}	0.0	7.5×10^{-4}	2.0×10^{-2}	2.0×10^{-2}	4.0×10^{-3}	4.0×10^{-3}
Tumor	0.80[a]	0.16[a]	0.80[a]	0.16[a]	10	10	1	1

*Specific binding forward rate constant for tumor, $k^{f,sp}$ min^{-1} · ml/pmol; nonspecific k^f taken as zero, with $k^{r,sp}$ = 0.0085 min^{-1}, and B_{max} for tumor taken as 1.18×10^{-8} M for IgG and F(ab')$_2$. BFA–hapten binding forward rate constant 5.6×10^9 M^{-1} · min^{-1}; reverse rate constant, 1.2 min^{-1}; streptavidin–biotin binding forward rate constant, 4.2×10^9 M^{-1} · min^{-1}; reverse rate constant, 5.4×10^{-6} min^{-1}.

TABLE 4
Calculated Radiation Doses by Two Different Methods

Method	Radionuclide	Bone	Kidney	Liver	Lung	Muscle	Skin	Spleen	Tumor	Gastrointestinal tract
Estimation using curve-fitting method										
	67Cu	0.56	2.30	0.94	0.68	0.017	0.46	0.57	1.80	0.53
	131I	1.10	5.10	2.20	1.30	0.63	1.00	1.21	3.10	1.10
	188Re	0.88	4.00	1.70	1.50	0.41	0.84	1.20	3.00	0.93
	90Y	2.40	13.00	4.90	3.70	1.20	2.60	2.90	7.30	2.70
Prediction using physiologically based pharmacokinetic model										
	67Cu	0.53	2.00	1.20	0.90	0.019	0.53	0.35	1.20	0.54
	131I	1.00	4.20	2.60	1.80	0.46	0.96	0.77	2.80	1.10
	188Re	0.97	4.10	2.50	1.90	0.35	1.30	0.73	2.10	1.20
	90Y	2.30	12.00	6.40	5.00	0.96	3.00	1.70	6.50	2.80

The table heading "Radiation dose (cGy/mCi)" spans all dose columns.

cally based pharmacokinetic model to validate the model for absorbed dose estimation.

Optimal Bifunctional Antibody Doses

The optimal antibody doses have been previously determined under the same baseline conditions for anti-CEA murine antibody ZCE025 (20). They were used as the optimal antibody doses for the preinjected anti-CEA BFA in this study [i.e., 14 mg/0.09 μmole for IgG and 10 mg/0.10 μmole for F(ab')$_2$] to achieve high tumor-specific antibody uptakes (20).

Injection Interval and Forced Antibody Clearance

Previous studies have shown that longer injection intervals lead to higher tumor-to-background effector agent uptake ratio as antibodies are cleared from the plasma and other normal tissues (20,21,25). Prolonged intervals, however, may not be feasible clinically. As an alternative, antibodies are frequently cleared out from the systemic circulation before effector agent administration with, for example, a polyvalent "chase" macromolecule. Here, two different injection intervals, a short interval of 3 days (72 hr) and a long interval of 20 days (480 hr) were considered, with and/or without prior "forced antibody clearance" (i.e., antibody concentration in plasma was set to zero before effector agent administration but was allowed to rise as material returned to the plasma from extravascular space). The potential benefits of "extended plasmapheresis" (continuous removal of all circulating free antibodies and maintaining zero plasma concentration) was also simulated as a part of our sensitivity analysis (see "Results").

Dose-Dependent Effector Agent Uptake and Optimal Effector Agent Doses

The hapten uptake in tumor (percentage injected dose per g of tissue) was simulated at a wide range of effector agent doses. The accumulated activities in tumor for 131I-labeled effector agent in both systems were then calculated as a function of effector agent dose. The optimal effector agent doses were selected as the doses that achieve 98% or higher of the maximum accumulated activities in tumor.

Radioimmunodetection

The tumor-to-liver effector agent uptake ratio was simulated as a function of time with the optimized protocols because the tumor-to-background uptake ratio is the most critical parameter in cancer detection (26–28). This enables us to discern the optimal antibody forms, to determine the earliest feasible imaging time and to assess the potential and limitations of the strategy.

Radioimmunotherapy

The feasibility of RAIT with tumor pretargeting was assessed by estimating the maximum achievable absorbed doses in tumor. Similar to direct targeting with antibodies, we chose the tumor-to-

bone marrow and tumor-to-liver absorbed dose ratios as the therapeutic ratios. The maximum achievable absorbed doses in tumor were the products of the maximum therapeutic ratios and the tolerable absorbed doses of the dose-limiting organs (3.0 Gy for bone marrow and 13.0 Gy for liver) (20).

Sensitivity Analysis

For any kinetic model, it is important to determine the impact that each parameter may have on the model due to its variability and uncertainty. For this purpose, the relative sensitivity coefficients of model parameters were calculated as $\Delta R/R$ as compared to $\Delta P/P$, i.e., the percentage change in tumor-to-bone marrow therapeutic ratio, R, as compared to the percentage change in parameter value, P. Positive values for the relative sensitivity mean that the therapeutic ratio increases when the parameter value increases, whereas negative values mean the opposite. A very small absolute value indicates that the therapeutic ratio is insensitive to that parameter.

Sensitivity analysis was also used to evaluate alternative drug administration schemes, antigen distributions and antibody–effector agent interaction. Specifically, we examined:

1. The impact of antigen expression in bone marrow;
2. The effect of shed tumor antigen;
3. The benefit of effector agent continuous infusion over bolus injection;
4. Antibody clearance by extended plasmapheresis; and
5. The optimal range of the binding affinity between the BFA and effector agent.

RESULTS

The success of tumor pretargeting relies on numerous interacting parameters that determine the effector agent uptake in tumor and critical normal tissues. The physiologically based pharmacokinetic model offers us a unified framework to quantitatively elucidate the impact of these parameters.

Absorbed Dose Estimation

The absorbed doses estimated using two different pharmacokinetic methods (i.e., empirical pharmacokinetics by curve fitting and physiologically based model-predicted pharmacokinetics) are listed in Table 4 for the BFA–hapten system. The comparison showed that the discrepancies between the model prediction (using no adjustable parameters) and the estimation with the curve fitting (from 10% to 80%) were within the variations associated with the clinical pharmacokinetics. Although introducing adjustable parameters to account for patient variability would give more accurate estimates, such an effort is not warranted at present considering the relatively large errors associated with experimental data.
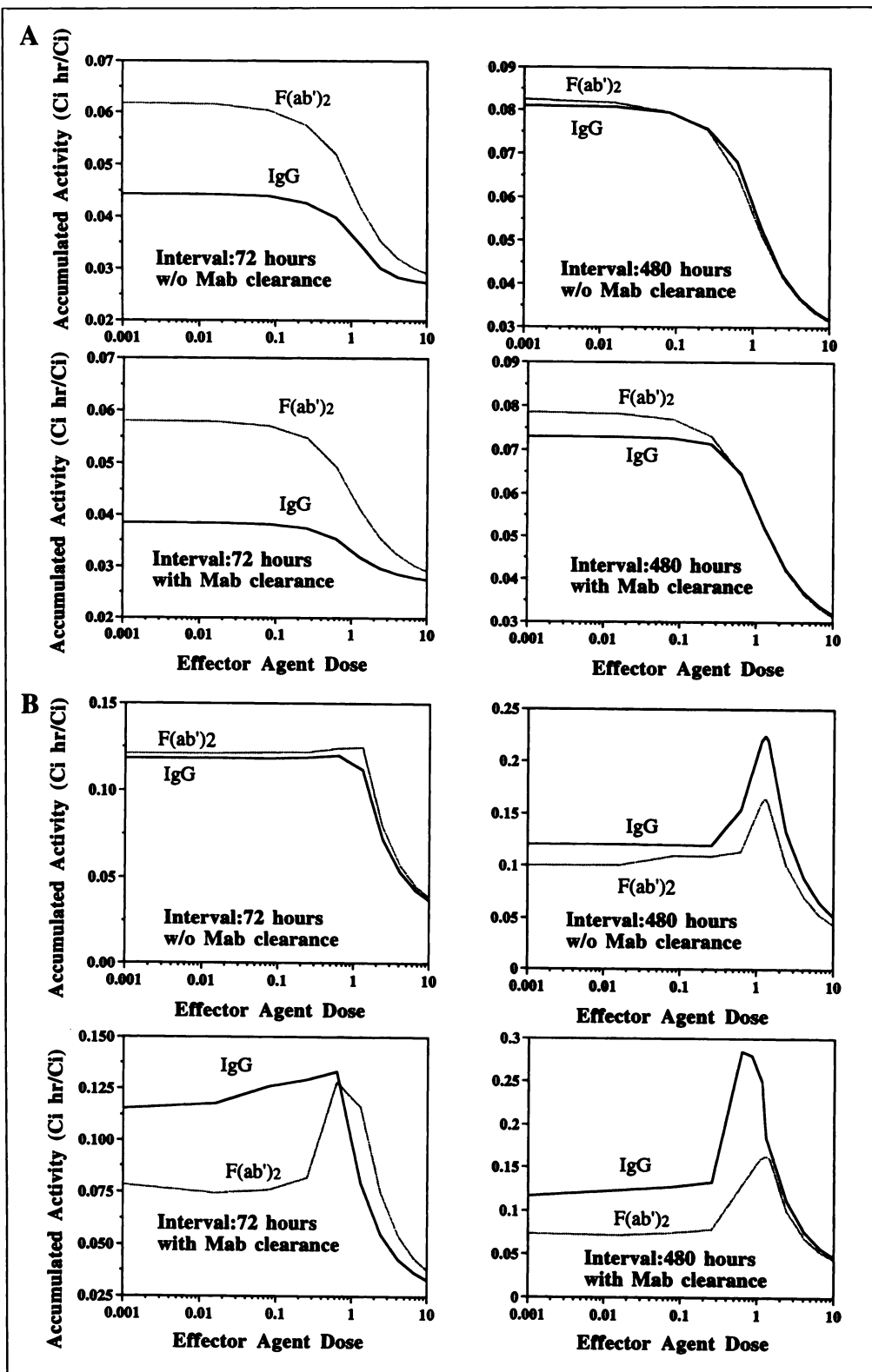
FIGURE 2. The accumulated activity for ^{131}I-labeled effector agent in humans as a function of hapten injection dose (relative to antibody molar dose) for different injection intervals, 72 hr and 480 hr, with and/or without forced antibody clearance from the systemic circulation before effector agent injection for the BFA–hapten (A) and streptavidinylated antibody–biotin (B) systems. Optimal BFA doses [14 mg for IgG and 10 mg for F(ab')₂] were used in the simulation. The optimal hapten injection dose was chosen to attain a relative accumulated activity in tumor of 98% of maximum.

Dose-Dependent Effector Agent Uptake and Optimal Effector Agent Doses

The accumulated activities in tumor are shown in Figure 2 as a function of effector agent dose for ^{131}I-labeled effector agent in the BFA–hapten and streptavidinylated antibody–biotin systems. The optimal effector agent doses were chosen as 20% of the antibody molar dose in the BFA–hapten system and 100% in the streptavidin-biotin system, for both IgG and F(ab')₂, with and/or without prior forced antibody clearance.

(These doses were based on the knee in the activity compared to dose curves in Fig. 2.)

The model simulations revealed a different effector agent dose dependence for the accumulated tumor activity in these two different systems. This was the result of the binding affinity differences between the BFAs and the effector agents. At very high binding affinity such as for the streptavidinylated antibody–biotin system, a large quantity of effector agent molecules was needed to first saturate the circulating free antibodies
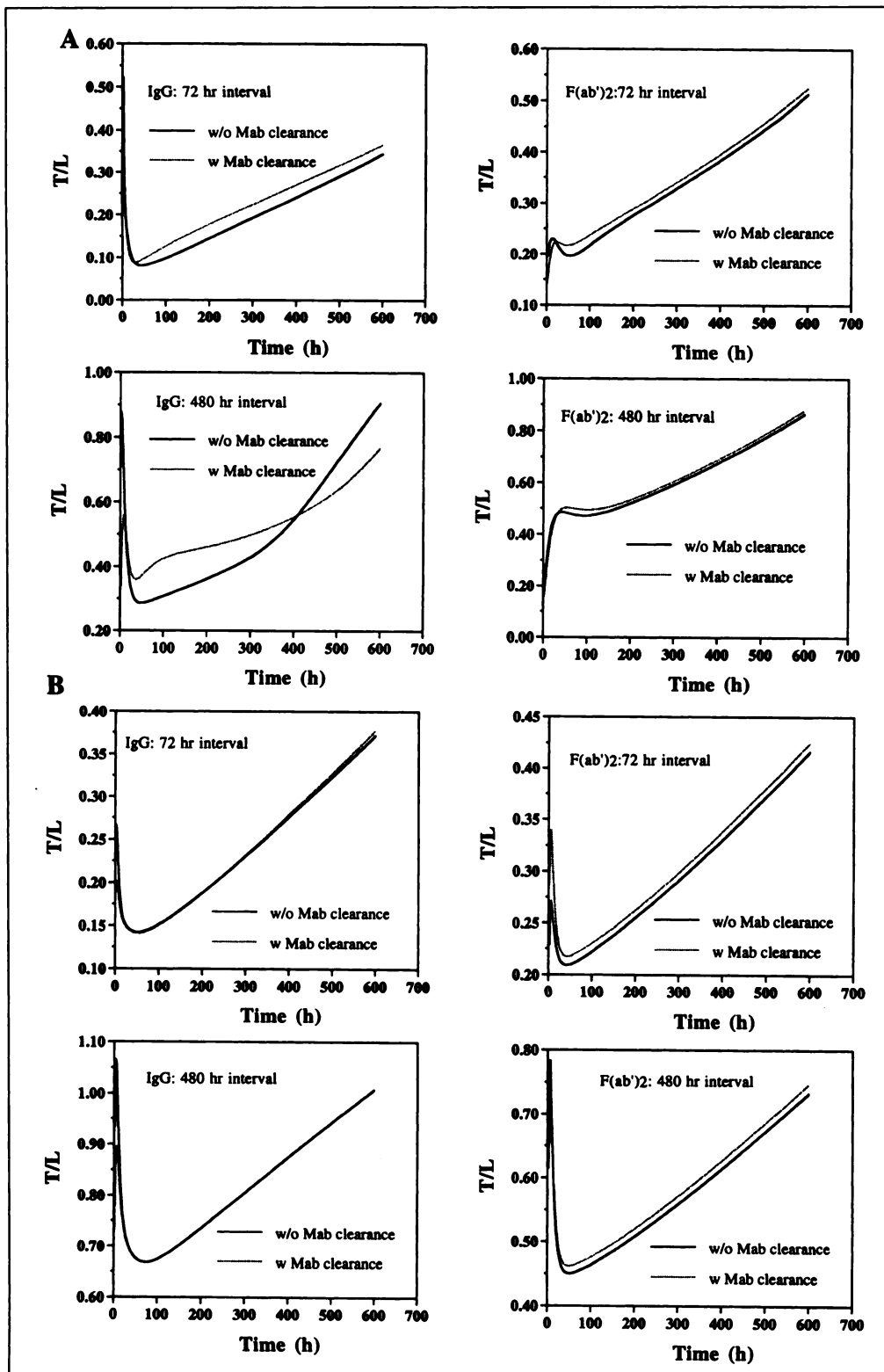
FIGURE 3. The tumor-to-liver uptake ratio as a function of time in humans for different injection intervals, 72 hr and 480 hr, with and/or without forced antibody clearance from the systemic circulation before effector agent injection for the BFA–hapten (A) and the streptavidinylated antibody-biotin (B) systems.

before they penetrated and bound with the BFAs inside the tumor.

Radioimmunodetection

The tumor-to-liver effector agent uptake ratio was simulated as a function of time for the BFA–hapten and streptavidinylated antibody–biotin systems (Fig. 3). After an early distribution phase, the tumor-to-liver uptake ratios were relatively low (<1.0). As antibodies were further excreted from normal tissues, the ratios increased as a result of antibody-specific binding in tumor. F(ab')$_2$ gave slightly higher uptake ratios than

did IgG in the BFA–hapten system, whereas IgG gave slightly higher uptake ratios than did F(ab')$_2$ in the streptavidinylated antibody–biotin system. Because the ratios were relatively high during the early distribution phase, an early imaging time (i.e., first 4 hr) was recommended.

Radioimmunotherapy

The absorbed doses and therapeutic ratios were calculated for a different combination of radionuclides (^{67}Cu, ^{90}Y, ^{131}I and ^{188}Re) and antibody forms [IgG and F(ab')$_2$] for the BFA–

TABLE 5
Absorbed Dose and Therapeutic Ratio for BFA–Hapten and Streptavidin–Biotin Systems*

System	Radionuclide	Tumor dose (cGy/mCi)	IgG tumor/BM	Tumor/liver	Tumor dose (cGy/mCi)	F(ab')$_2$ Tumor/BM	Tumor/liver
BFA–hapten	^{67}Cu	0.77 (0.71)	2.57 (2.88)	0.23 (0.23)	0.95 (0.92)	2.23 (2.32)	0.30 (0.30)
	^{131}I	3.37 (2.84)	3.60 (3.80)	0.36 (0.36)	3.16 (2.96)	3.30 (3.37)	0.42 (0.43)
	^{188}Re	0.90 (0.80)	2.04 (2.34)	0.15 (0.15)	1.19 (1.14)	1.71 (1.73)	0.22 (0.22)
	^{90}Y	2.25 (2.09)	1.99 (2.27)	0.13 (0.13)	3.56 (3.45)	2.02 (2.10)	0.22 (0.22)
Strepatividinylated antibody–biotin	^{67}Cu	1.26 (1.05)	2.55 (2.82)	0.26 (0.31)	1.51 (1.41)	3.55 (3.67)	0.32 (0.33)
	^{131}I	7.97 (5.73)	3.46 (3.63)	0.41 (0.45)	8.76 (7.92)	4.66 (4.71)	0.46 (0.47)
	^{188}Re	1.11 (1.03)	2.09 (3.03)	0.19 (0.29)	1.42 (1.48)	3.01 (3.34)	0.24 (0.27)
	^{90}Y	4.35 (4.04)	2.15 (2.64)	0.17 (0.22)	5.91 (5.67)	3.46 (3.68)	0.23 (0.25)

BM = bone marrow.
*Numbers in parentheses are calculated with forced antibody clearance from plasma.

hapten and streptavidinylated antibody–biotin systems (Table 5).

For the BFA–hapten system, ^{131}I-labeled hapten with IgG gave the highest tumor-to-bone marrow therapeutic ratio of 3.80, and ^{131}I-labeled hapten with F(ab')$_2$ gave the highest tumor-to-liver therapeutic ratio of 0.43, with prior forced antibody clearance. For the streptavidinylated antibody–biotin system, a moderately higher tumor-to-bone marrow therapeutic ratio of 4.71 and a tumor-to-liver therapeutic ratio of 0.47 were achieved for ^{131}I-labeled biotin with F(ab')$_2$ with prior forced antibody clearance. Consequently, the maximum achievable absorbed dose in tumor was 14.13 Gy when bone marrow toxicity was the limiting factor under the baseline physiological conditions.

The results indicated that 3%–10% increases in therapeutic ratios were achieved with prior antibody clearance. These moderate improvements, consistent with certain experimental observations (29), were mainly due to the return of the BFA to the plasma from normal tissues.
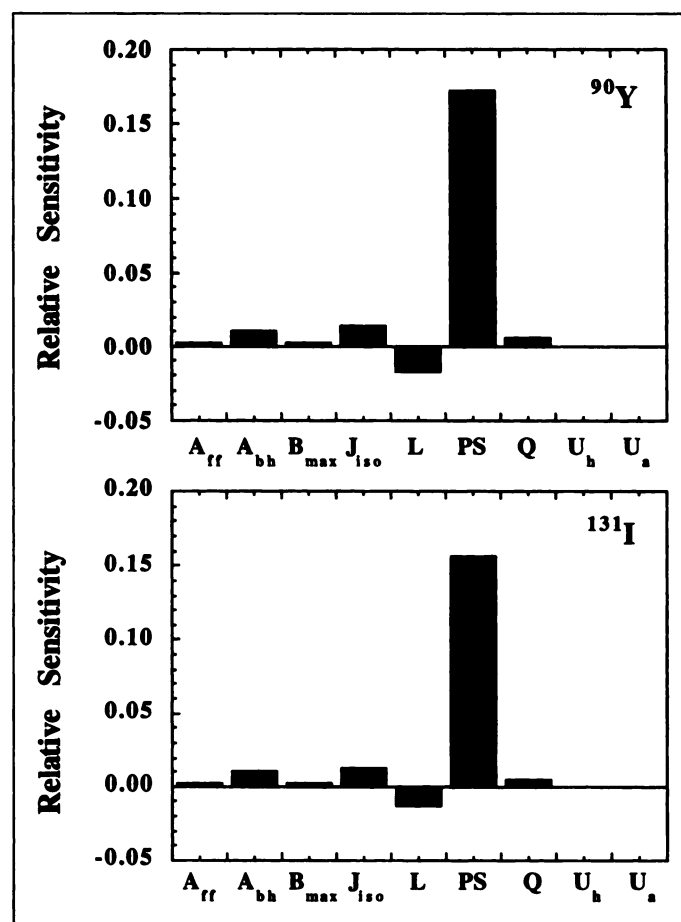
Sensitivity Analysis

The sensitivity coefficients are given in Figure 4 for ^{90}Y- and ^{131}I-labeled hapten with IgG in the BFA–hapten system. Tumor vascular permeability, tumor fluid recirculation rate and tumor fluid drainage were the most important parameters determining uptake, whereas moderate changes in tumor plasma flow rate, antibody–effector agent affinity and antibody-antigen affinity have minimal effect on the therapeutic ratios.

The sensitivity analysis suggested that further increasing the BFA–effector agent affinity from 10^9 M^{-1} (baseline value) to 10^{10} M^{-1} led to a 9.0% increase in tumor-to-bone marrow absorbed dose ratio for ^{131}I and a 11.0% for ^{90}Y-labeled hapten, whereas increasing the affinity from 10^{10} M^{-1} to 10^{11} merely led to a 1.1% increase for ^{131}I and a 1.2% increase for ^{90}Y-labeled hapten in the BFA–hapten system. Continuous infusion of the effector agent for 3 days resulted in a limited (4.1%) increase in tumor-to-bone marrow therapeutic ratio for ^{131}I and 3.3% for ^{90}Y.

Our analysis demonstrated that an antigen expression level in bone marrow as high as 10% of that in the tumor resulted in only a 0.4% increase for ^{90}Y and 0.7% for ^{131}I in absorbed dose in bone marrow with minimal impact on the therapeutic ratios. Tumor antigen shedding reduced the tumor absorbed dose by only 0.2% for ^{131}I and 0.4% for ^{90}Y at a high turnover rate of 1 hr.

Because one-time clearance of antibody from the plasma had only a small increase in therapeutic ratio, we wanted to see if continuous removal of antibody could be more effective. This would also remove any unbound antibody returning to the

bloodstream from normal tissues (mathematically the antibody plasma concentration may be set to zero instantaneously or maintained at zero for some duration). Using extended plasmapheresis (continuous clearance) to remove all of the free antibody from the systemic circulation, a significant improvement in tumor-to-liver uptake ratio (a 10-fold increase) may be achieved in RAID (Fig. 5) and up to a 117% increase in the therapeutic ratio may be achieved for short-lived ^{90}Y labeled hapten in the BFA–hapten system. However, only a limited (2.8%) increase was achieved for ^{131}I-labeled hapten because

FIGURE 4. The sensitivity analysis for ^{90}Y- and ^{131}I-labeled effect agents in combination with bifunctional IgG in BFA–hapten system for tumor plasma flow rate (Q), tumor lymphatic flow rate (L), tumor fluid recirculation rate (J$_{iso}$), tumor vascular permeability PS (both large and small pores) for antibody, tumor antigen expression (B$_{max}$), antibody-antigen binding affinity (A$_{ff}$), antibody–agent binding affinity (A$_{bh}$) and urine excretion rate (U$_{x=a,h}$) for the BFA and the hapten.
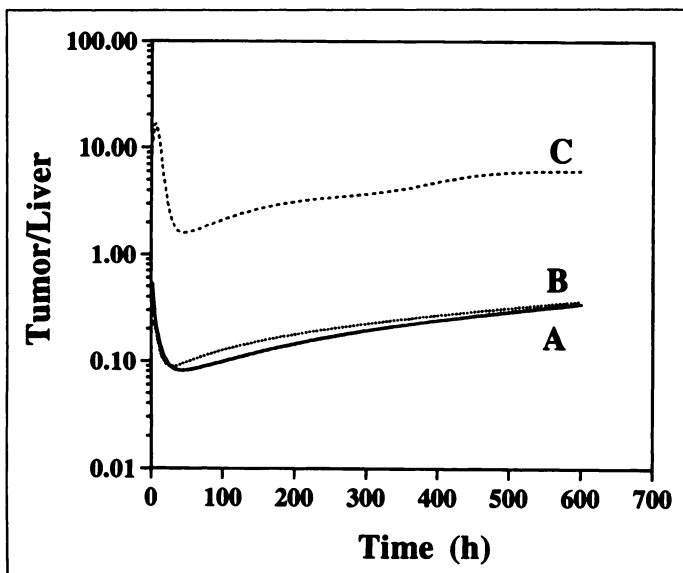
FIGURE 5. Comparison of different antibody clearance schemes in the BFA (IgG)–hapten system without forced antibody clearance (A), with forced antibody before effector agent administration (B) and with continuous removal of free circulating antibody (C).

the dramatically increased antibody clearance diminished the benefit of long-lived radionuclides. The small improvement of one-time plasma clearance in Figure 5 is due to return of antibody from all normal tissues to the bloodstream and the blood's small percentage of body weight in humans, i.e., only a small fraction of total antibody in the body is removed by instantaneous clearance of BFA in the blood.

DISCUSSION

The mathematical model for antibody pharmacokinetics and dosimetry calculations has helped us to understand the transport barriers to multistep methods using monoclonal antibodies. This information was used to address the potential of tumor pretargeting for RAID and RAIT under more favorable conditions.

Important Model Parameters and Physiological Barriers

Sensitivity analysis showed that antibody extravasation is the major determinant for BFA accumulation and, thus, the effector agent accretion in tumor. Modulating tumor vascular permeability would thus be most beneficial to improved effector agent delivery (30–32).

The antibody–antigen binding affinity and antibody–effector agent binding affinity were expected to affect to the tumor-to-background ratio (33). The model found these two affinities to have moderate impact on the therapeutic ratios with limited gains from very high affinities. This suggested that the usefulness of increasing the binding affinities beyond the baseline level (10^{10} M^{-1}) to improve effector agent selectivity would be limited by physiological barriers. The streptavidinylated antibody–biotin system, characterized with high antibody–effector agent binding affinity, thus did not result in more significant advantages over the BFA–hapten system.

Cancer Detection with Tumor Pretargeting: Limitations and Potential

Tumor pretargeting was found to be capable of achieving 200% higher tumor-to-background ratio than was direct antibody targeting, under the same baseline tumor physiological conditions, with the greatest improvement in the early period. Antibody clearance from the plasma before effector agent administration or prolonged injection interval was expected to

improve the strategy, but it only resulted in a moderate increase of 3%–10%. Thus, the highest tumor-to-background uptake ratio remained relatively low (about 1.0) for typical solid tumors, even using the optimized protocols in both pretargeting systems. For the gamma-ray camera, using the subtraction method, a ratio of approximately 2.5 is required for the hypothetical 20-g tumor (i.e., 1.7-cm diameter) at 5-cm depth (28). This suggests that solid tumors at difficult sites, such as hepatic metastases, are unlikely to be detected. The role of tumor pretargeting in cancer diagnosis may thus be less than anticipated because hepatic metastases are among the most common for colorectal cancers (1).

It is important to note that tumor physiology is highly variable and depends strongly on tumor type, size, stage and host tissue. Sensitivity analysis indicated that tumor-to-background uptake ratio could be increased for tumors with favorable physiological conditions (i.e., increased vascular permeability). For example, the analysis indicated that a 2.6-fold increase in tumor-to-background uptake ratio would be achieved in tumors with 6-fold higher permeability than the baseline value (Fig. 4). This would permit the detection of such tumors in the early period after the effector agent administration. Screening cancer patients for proper tumor types, stages and other physiological parameters (e.g., vascular endothelial growth factor concentration) that correlate with tumor vascular permeability may help to improve the effectiveness of the strategy.

Besides taking advantage of the physiological variations among solid tumors, more drastic measures, such as extended plasmapheresis removing all free antibody from the systemic circulation, were shown to significantly increase the tumor-to-background uptake ratio and make detection feasible even under typical tumor physiological conditions.

Cancer Therapy with Tumor Pretargeting: Limitations and Potential

Using the optimized protocols, the maximum achievable absorbed dose in tumor was only 14.13 Gy under the baseline tumor physiological conditions. Under favorable tumor conditions, with 6-fold higher vascular permeability, a greatly increased absorbed dose in tumor of 28.5 Gy was achievable. However, the 60%–70% tumor control dose for majority of carcinomas of aerodigestive tract (lung, stomach, liver and gastrointestinal tract) is about 35 Gy with external beam irradiation (34). Although the radiobiological criterion derived from external beam irradiation may not be fully applicable, this suggests that RAIT with tumor pretargeting was inadequate as the sole therapeutic modality for solid tumor even using optimized protocols under favorable tumor physiological conditions.

Using drastic measures such as extended plasmapheresis, a 30.7-Gy absorbed dose for typical solid tumors was achievable but still less than the required tumor control dose. Only in tumors with favorable conditions will RAIT be feasible for substantial tumor control using extended plasmapheresis. An estimated absorbed dose of 61.8 Gy could be achieved in tumor.

Comparison with Previous Studies

We compared our major conclusions with previously published studies in the literature as an evaluation of the physiologically based pharmacokinetic model (Table 6).

Yuan et al. (35) were among the first to determine optimal conditions for tumor pretargeting and assess its advantages over direct tumor targeting. Baxter et al. (21) further optimized the tumor pretargeting protocols based on a physiologically based pharmacokinetic model. Similar efforts have also been made

TABLE 6
Comparison of Different Pharmacokinetic Analyses

	Pharmacokinetic model/study	Tumor and system	Optimal BFA dose/form	Optimal injection interval	Optimal effector agent doses	Optimal BFA–agent affinity	Desirable radionuclides
Compartmental pharmacokinetics	Yuan et al. (35)	N/A BFA–hapten Human	BFA IgG 10^{-8} M	As long as possible	100% antibody molar dose	10^9 M^{-1}	N/A
	Baxter et al. (21)	20-g tumor BFA–hapten Human	BFA F(ab')$_2$ 10^{-7} M	10% antibody molar dose	10% antibody molar dose	10^{11} M^{-1}	[131]I and [90]Y
Distributed pharmacokinetics	Sung and van Osdol (36)	0.014-g tumor Streptavidin–biotin Human	BFA IgG 50–200 nM (23–90 mg)	72 hr	50% antibody molar dose	10^{15} M^{-1}	N/A
Clinical observations	Goodwin et al (10)	BFA–hapten Mouse	BFA IgG/50 μg	21 hr	0.3–1.0 nmol	10^7–10^8 M^{-1}	N/A
	Yao et al. (29)	Biotin–avidin Mouse	BFA IgG/30μg	48 hr	3 μg	10^{15} M^{-1}	N/A

N/A = not applicable.

using distributed models (18,36). The present model was in agreement with other theoretical analyses, with certain quantitative discrepancies, because of the different baseline conditions. The strength of the present model lies in the ability to address these issues in a integrated way and in use of measurable physiological parameters for greater reliability.

Model Limitations

The model analysis was based on the pharmacokinetics of BFA and hapten in a standard patient under average tumor physiological conditions. It did not fully address the variability that is associated with tumor, nor did it include the impact of tumor modulation, chemical link and the fate of lost labels, alternative antigen targets and alternative antibody constructs. There are certain limitations with the model assumptions, and special caution must be taken to interpret the results.

The model assumed a fixed-size hypothetical tumor with constant antigen concentration. The simulations were, thus, the averaged effects without considering tumor growth or regression during treatment and heterogeneity among different tumors. For example, sensitivity analysis found that plasma flow rate to tumor was not a sensitive parameter. However, in heterogeneous tumor vasculature increasing blood flow rate and/or making perfusion more uniform may change the distribution pattern, i.e., open new pathways. This would serve to increase the tumor vascular permeability–surface area product, which would improve delivery of the effector agent to tumor.

Another assumption was the uniform BFA distribution within tissue. This is a feature of lumped pharmacokinetic models. This is a good approximation for low molecular weight agents; however, the distribution is heterogeneous for macromolecules (7). Under significantly elevated vascular permeability, the antibody distribution may be limited by its diffusion in the extracellular matrix. Distributed models and microdosimetric methods must be developed to evaluate such effects. For beta-emitting radionuclides with a range of a few millimeters and for small tumors, the assumption is, nevertheless, reasonable under the time scale of interest especially for micrometastases, the primary targets of RAID and RAIT.

Although there was general agreement between the model estimates (predictions based on physiological parameters alone) and the doses calculated from clinical data, we are not suggesting that the model be used for accurate prediction of dose in patients. Given the assumptions described above and the variability between patients, no model could make precise predictions based on average physiological parameters. Instead, approximate dose predictions have been shown to be possible using the model with good potential for describing relative changes in dose obtained by changing protocols or materials. The data comparison and the hapten parameters are based on a single BFA–hapten system (17,21). Further validation of the model with direct dosimetry measurements compared to model simulations using individualized patient parameters and various antibody–hapten combinations would be beneficial.

CONCLUSION

The physiologically based pharmacokinetic model provided a useful method to obtain initial estimates of the absorbed doses for the tumor pretargeting systems in the absence of clinical data and has potential in the clinical treatment planning process. The model analysis suggested that tumor pretargeting provided a definite advantage over direct antibody targeting with up to a 200% increase in tumor-to-background ratio in RAID and up to a 76% increase in tumor-to-bone marrow therapeutic ratio in RAIT. With the optimized protocols for typical cancer patients, the model showed that biotin with the streptavidinylated IgG provided the highest tumor-to-background ratio in RAID, and ^{131}I-conjugated biotin with the streptavidinylated F(ab')$_2$ provided the highest therapeutic ratios in RAIT. Sensitivity analysis indicated that antibody extravasation into the tumor was the major limitation for the accretion of effector agent in tumor, whereas antigen expression in normal tissue and tumor antigen shedding had little effect on the absorbed doses. Hence, strategies to increase tumor permeability or to screen for patients with high tumor permeability may help increase the effectiveness. Despite the advantages of multistep methods, our analysis found that tumor pretargeting was not sensitive enough for detecting typical hepatic metastases and that tumor pretargeting was inadequate as the sole therapeutic modality in RAIT for patients with typical solid tumor physiological conditions, unless drastic measures, such as extended plasmapheresis, are used.

ACKNOWLEDGMENTS

APPENDIX A: NOMENCLATURE

$\tilde{A}_{organ}$	Accumulated activity in organ i (Ci·h/Ci)
B_{max}	Antigen concentration in tumor (M)
$C_{x\text{-}v,organ}$	BFA (x = a), effector agent (x = h) and their complex (x = ah) concentration in the vascular space (M)
$C^f_{x\text{-}i,organ}$	Free BFA (x = a), effector agent (x = h) and their complex (x = ah) concentrations in the interstitial space (M)
$C^b_{x\text{-}i,organ}$	Nonspecifically bound BFA (x = a), effector agent (x = h) and their complex (x = ah) concentration in the interstitial space (M)
$C^{fb}_{ab\text{-}i,organ}$	Antibody–antigen concentration in the interstitial space (M)
$C^{bf}_{ah\text{-}i,organ}$	Complex concentration from bound antibody with free agent in the interstitial space (M)
$C^{ff}_{ah\text{-}i,organ}$	Complex concentration from free antibody with free agent in the interstitial space (M)
$C^{fb}_{ah\text{-}i,organ}$	Complex concentration from free antibody with bound agent in the interstitial space (M)
$C^{ffb}_{ahb\text{-}i,organ}$	Antibody–antigen–agent concentration in the interstitial space (M)
D_{organ}	Absorbed dose in organ i (cGy/mCi)
$J_{iso,organ}$	Fluid recirculation flow rate (= flow rate through large pore into the interstitial space for L = 0) (ml/min)
$J_{S,organ}J_{L,organ}$	Transcapillary fluid flow rate (vascular → interstitial) for each organ via small and large pores, respectively (ml/min)
$J_{x,organ}$	Extravasation rate (transcapillary exhange rate) for BFA (x = a), effector agent (x = h) and the complex (x = ah) (moles/min)
$k_{EL,organ}$	Catabolic elimination rate (ml/min)
k^f, k^r	Association and disassociation constants for antibody–antigen ($k^{f,sp}M^{-1}\cdot min^{-1}$ and $k^{r,sp}min^{-1}$ for specific binding)
L_{organ}	Lymph flow rate (ml/min)
M_i	Mass organ i (g)
$PS_{x,organ}$	Permeability–surface area product for species x, per organ (ml/min)
Q_{organ}	Plasma flow rate (ml/min)
U_x	Excretion rate constants for the BFA (x = a), the therapeutic agent (x = h) and their complex (x = ah), respectively, via kidney urine clearance (ml/min)
$V_{i,organ}$	Organ interstitial space (ml)
$V_{v,organ}$	Organ vascular space (ml) (V_{pl} is total plasma volume)
$V_{T,organ}$	Total organ volume (ml)
Δ_{np}	Mean energy emitted per nuclear transition for particle i (np for nonpenetrating radiation) (g·cGy/μCi·h)
$\Phi_{i(dest\leftarrow src)}$	Specific absorption fraction of energy for target organ (dest) for particle i emitted in the source organ (src)
$\sigma_{x,L}, \sigma_{x,S}$	Osmotic reflection coefficients of large and small pores for BFA (x = a), effector agent (x = h) and their complex (x = ah)

APPENDIX B: MATHEMATICAL MODEL AND GOVERNING MASS BALANCE EQUATIONS

The mass balance equations for the pharmacokinetic model describe the circulation of the BFA, the therapeutic agent and their binding complex throughout the body (Fig. 1). The equations are solved using Livermore Solver of Ordinary Differential Equations with Gear's method for stiff equations (37). The extravasation of BFA (x = a), effector agent (x = h) and their complex (x = ah) are determined by the following equations according to the two pore model proposed by Rippe and Haraldsson (38,39):

$$J_{x,v\text{-}i} = J_{L,organ}(1 - \sigma_{L,x})C_{x\text{-}v,organ} + PS_{x\text{-}L,organ}(C_{x\text{-}v,organ}$$

$$- C^f_{x\text{-}i,organ}/R_{organ}) \frac{Pe_{x\text{-}L}}{e^{Pe_{x\text{-}L}} - 1} + J_{S,organ}(1 - \sigma_{S,x})C_{x\text{-}v,organ}$$

$$+ PS_{x\text{-}S,organ}(C_{x\text{-}v,organ} - C^f_{x\text{-}i,organ}/R_{organ}) \frac{Pe_{x\text{-}S}}{e^{Pe_{x\text{-}S}} - 1}$$

and

$$J_{L,organ} = J_{iso,organ} + \alpha_L L_{organ}; \quad J_{S,organ} = - J_{iso,organ} + \alpha_S L_{organ}.$$

For each organ subcompartment (vascular space, interstitial space and tumor-bound species in the interstitial space), mass balances are written In the vascular compartment, the rate of accumulation equals the rate entering via the bloodstream minus the rate leaving via the blood minus the rate of extravasation, accounting for any conversion between bound and unbound species In the interstitial

space. The accumulation rate is the rate of material entering from the plasma minus the rate it leaves via the lymph and the rates at which the materials becomes bound or unbound. For additional details, see refs. 20 and 21.

Mass Balance Equation for Plasma

$$V_{pl}(dC_{a\text{-}v,pl}/dt) = (Q_{lung} - L_{lung})C_{a\text{-}v,lung} + L_{lung}C^f_{a\text{-}i,lung}$$

$$+ L_{liver}C^f_{a\text{-}i,liver} + L_{gi}C^f_{a\text{-}i,gi} + L_{spleen}C^f_{a\text{-}i,spleen}$$

$$+ L_{kidney}C^f_{a\text{-}i,kidney} + L_{tumor}C^f_{a\text{-}i,tumor}$$

$$+ L_{skin}C^f_{a\text{-}i,skin} + L_{muscle}C^f_{a\text{-}i,muscle}$$

$$+ L_{bone}C^f_{a\text{-}i,bone} + L_{heart}C^f_{a\text{-}i,heart} - (Q_{liver}$$

$$+ L_{gi} + L_{spleen} + Q_{kidney} + Q_{tumor} + Q_{skin}$$

$$+ Q_{muscle} + Q_{bone} + Q_{heart})C_{a\text{-}v,pl}$$

$$- V_{pl}(K^f_{ah}C_{a\text{-}v,pl}C_{h\text{-}v,pl} - K^r_{ah} \cdot C_{ah\text{-}v,pl})$$

$$V_{pl}(dC_{h\text{-}v,pl}/dt) = (Q_{lung} - L_{lung})C_{h\text{-}v,lung} + L_{lung}C^f_{h\text{-}i,lung}$$

$$+ L_{liver}C^f_{h\text{-}i,liver} + L_{gi}C^f_{h\text{-}i,gi} + L_{spleen}C^f_{h\text{-}i,spleen}$$

$$+ L_{kidney}C^f_{h\text{-}i,kidney} + L_{tumor}C^f_{h\text{-}i,tumor}$$

$$+ L_{skin}C^f_{h\text{-}i,skin} + L_{muscle}C^f_{h\text{-}i,muscle}$$

$$+ L_{bone}C^f_{h\text{-}i,bone} + L_{heart}C^f_{h\text{-}i,heart} - (Q_{liver}$$

$$+ \ L_{gi} + L_{spleen} + Q_{kidney} + Q_{tumor} + Q_{skin}$$
$$+ \ Q_{muscle} + Q_{bone} + Q_{heart})C_{h-v,pl}$$
$$- \ V_{pl}(K^f_{ah}C_{a-v,pl}C_{h-v,pl} - K^r_{ah} \cdot C_{ah-v,pl})$$

$$V_{pl}(dC_{ah-v,pl}/dt) = (Q_{lung} - L_{lung})C_{ah-v,lung} + L_{lung}C^f_{ah-i,lung}$$
$$+ \ L_{liver}C^f_{ah-i,liver} + L_{gi}C^f_{ah-i,gi}$$
$$+ \ L_{spleen}C^f_{ah-i,spleen} + L_{kidney}C^f_{ah-i,kidney}$$
$$+ \ L_{tumor}C^f_{ah-i,tumor} + L_{skin}C^f_{ah-i,skin}$$
$$+ \ L_{muscle}C^f_{ah-i,muscle} + L_{bone}C^f_{ah-i,bone}$$
$$+ \ L_{heart}C^f_{ah-i,heart} - (Q_{liver} + L_{gi} + L_{spleen}$$
$$+ \ Q_{kidney} + Q_{tumor} + Q_{skin} + Q_{muscle} + Q_{bone}$$
$$+ \ Q_{heart})C_{ah-v,pl} + V_{pl}(K^f_{ah}C_{a-v,pl}C_{h-v,pl}$$
$$- \ K^r_{ah} \cdot C_{ah-v,pl})$$

There is an additional constraint on the volumetric flow rates:

$$Q_{lung} = Q_{liver} - L_{liver} + Q_{kidney} - L_{kidney} + Q_{tumor} - L_{tumor}$$
$$+ \ Q_{skin} - L_{skin} + Q_{muscle} - L_{muscle} + Q_{bone} - L_{bone}$$
$$+ \ Q_{heart} - L_{heart}$$

Mass Balance Equations for Lung
For vascular space:

$$V_{v,lung}(dC_{x-v,lung}/dt) = (Q_{liver} - L_{liver})C_{x-v,liver} +$$
$$(Q_{kidney} - L_{kidney})C_{x-v,kidney} +$$
$$(Q_{tumor} - L_{tumor})C_{x-v,tumor} +$$
$$(Q_{skin} - L_{skin})C_{x-v,skin} +$$
$$(Q_{muscle} - L_{muscle})C_{x-v,muscle} +$$
$$(Q_{bone} - L_{bone})C_{x-v,bone} +$$
$$(Q_{heart} - L_{heart})C_{x-v,heart} -$$
$$(Q_{lung} - L_{lung})C_{x-v,lung} - J_{x,lung}$$
$$- \ V_{v,lung}(K^f_{ah}C_{a-v,lung}C_{h-v,lung}$$
$$- \ K^r_{ah} \cdot C_{ah-v,lung})$$

$$V_{v,lung}(dC_{ah-v,lung}/dt) = (Q_{liver} - L_{liver})C_{ah-v,liver} +$$
$$(Q_{kidney} - L_{kidney})C_{ah-v,kidney} +$$
$$(Q_{tumor} - L_{tumor})C_{ah-v,tumor} +$$
$$(Q_{skin} - L_{skin})C_{ah-v,skin} +$$
$$(Q_{muscle} - L_{muscle})C_{ah-v,muscle} +$$
$$(Q_{bone} - L_{bone})C_{ah-v,bone} +$$
$$(Q_{heart} - L_{heart})C_{ah-v,heart} -$$
$$(Q_{lung} - L_{lung})C_{ah-v,lung} - J_{ah,lung}$$
$$+ \ V_{v,lung}(K^f_{ah}C_{a-v,lung}C_{h-v,lung}$$
$$- \ K^r_{ah}C_{ah-v,lung})$$

Mass Balance Equations for Liver
For vascular space:

$$V_{v,liver}(dC_{x-v,liver}/dt) = (Q_{gi} - L_{gi})C_{x-v,gi} + (Q_{spleen}$$
$$- \ L_{spleen})C_{x-v,spleen} + (Q_{liver} - Q_{gi} - Q_{spleen}$$

$$+ \ L_{gi} + L_{spleen})C_{x-v,pl} -$$
$$(Q_{liver} - L_{liver})C_{x-v,liver} - J_{x,liver}$$
$$- \ V_{v,liver}(K^f_{ah}C_{a-v,liver}C_{h-v,liver} - K^r_{ah}C_{ah-v,liver})$$

$$V_{v,liver}(dC_{ah-v,liver}/dt) = (Q_{gi} - L_{gi})C_{ah-v,gi} + (Q_{spleen}$$
$$- \ L_{spleen})C_{ah-v,spleen} + (Q_{liver} - Q_{gi}$$
$$- \ Q_{spleen} + L_{gi} + L_{spleen})C_{ah-v,pl} -$$
$$(Q_{liver} - L_{liver})C_{ah-v,liver} - J_{ah,liver}$$
$$+ \ V_{v,liver}(K^f_{ah}C_{a-v,liver}C_{h-v,liver} - K^r_{ah}C_{ah-v,liver})$$

Mass Balance Equations for Kidney
For vascular space:

$$V_{v,kidney}(dC_{x-v,kidney}/dt) = Q_{kidney}C_{x-v,pl} - (Q_{kidney} - L_{kidney})C_{x-v,liver}$$
$$- \ U_xC_{x-v,kidney} - J_{x-v}$$
$$- \ V_{v,kidney}(K^f_{ah}C_{a-v,kidney}C_{h-v,kidney}$$
$$- \ K^r_{ah}C_{ah-v,kidney})$$

$$V_{v,kidney}(dC_{ah-v,kidney}/dt) = Q_{kidney}C_{ah-v,pl} - (Q_{kidney}$$
$$- \ L_{kidney})C_{ah-v,liver} - U_{ah}C_{ah-v,kidney}$$
$$- \ J_{ah-v} + V_{v,kidney}(K^f_{ah}C_{a-v,kidney}C_{h-v,kidney}$$
$$- \ K^r_{ah}C_{ah-v,kidney})$$

Mass Balance Equations for Tumor and Other Organs
For vascular space:

$$V_{v,organ}(dC_{a-v,organ}/dt) = Q_{organ}C_{a-v,pl} - (Q_{organ} - L_{organ})C_{a-v,organ}$$
$$- \ J_{a,organ} - V_{v,organ}(K^f_{ah}C_{a-v,organ}C_{h-v,organ}$$
$$- \ K^r_{ah}C_{ah-v,organ})$$

$$V_{v,organ}(dC_{h-v,organ}/dt) = Q_{organ}C_{h-v,pl} - (Q_{organ} - L_{organ})C_{h-v,organ}$$
$$- \ J_{h,organ} - V_{v,organ}(K^f_{ah}C_{a-v,organ}C_{h-v,organ}$$
$$- \ K^r_{ah}C_{ah-v,organ})$$

$$V_{v,organ}(dC_{ah-v,organ}/dt) = Q_{organ}C_{ah-v,pl} - (Q_{organ} - L_{organ})C_{ah-v,organ}$$
$$- \ J_{ah,organ} + V_{v,organ}(K^f_{ah}C_{a-v,organ}C_{h-v,organ}$$
$$- \ K^r_{ah}C_{ah-v,organ})$$

For interstitial space:

$$V_{i,organ}(dC^f_{a-i,organ}/dt) = J_{a,organ} - L \cdot C^f_{a-i,organ}$$
$$- \ V_{i,organ} \cdot (K^f_{a,organ}C^f_{a-i,organ}$$
$$- \ K^r_{a,organ}C^b_{a-i,organ})$$
$$- \ V_{i,organ} \cdot (K^f_{ah}C^f_{a-i,organ}(C^f_{h-i,organ}$$
$$+ \ C^b_{h-i,organ})) + V_{i,organ} \cdot (K^r_{ah}(C^{ff}_{ah-i,organ}$$
$$+ \ C^{fb}_{ah-i,organ})) - V_{i,organ} \cdot (K^f_{ab}(B_{max}$$
$$- \ C^{fb}_{ab-i,organ} - C^{ffb}_{ahb-i,organ}) \cdot C^f_{a-i,organ}$$
$$- \ K^r_{AB}C^{fb}_{ab-i,organ})$$

$$V_{i,organ}(dC^b_{a-i,organ}/dt) = V_{i,organ} \cdot (K^f_{A,organ}C^f_{a-i,organ} - K^r_{A,organ}C^b_{a-i,organ})$$
$$- \ V_{i,organ} \cdot (K^f_{ah}C^b_{a-i,organ} \cdot C^f_{h-i,organ}$$
$$- \ K^r_{ah}C^{bf}_{ah-i,organ})$$

$$V_{i,organ}(dC^{fb}_{ab-i,organ}/dt) = V_{i,organ}(K^f_{ab}(B_{max} - C^{fb}_{ab-i,organ}$$

$$- C^{ffb}_{ahb-i,organ})C^f_{a-i,organ} - K^r_{ab}C^{fb}_{ab-i,organ})$$

$$- V_{i,organ} \cdot (K^f_{ah}C^f_{h-i,organ}C^{fb}_{ab-i,organ}$$

$$- K^r_{ah}C^{ffb}_{ahb-i,organ})$$

$$V_{i,organ}(dC^f_{h-i,organ}/dt) = J_{h,organ} - L \cdot C^f_{h-i,organ}$$

$$- V_{i,organ} \cdot (K^f_{h,organ}C^f_{h-i,organ}$$

$$- K^r_{h,organ}C^b_{h-i,organ})$$

$$- V_{i,organ} \cdot (K^f_{ah}C^f_{h-i,organ}(C^f_{a-i,organ}$$

$$+ C^b_{a-i,organ}) - K^r_{ah}(C^{ff}_{ah-i,organ} + C^{bf}_{ah-i,organ}))$$

$$- V_{i,organ} \cdot (K^f_{ah}C^f_{h-i,organ}C^{fb}_{ab-i,organ}$$

$$- K^r_{ah}C^{ffb}_{ahb-i,organ})$$

$$V_{i,organ}(dC^b_{h-i,organ}/dt) = V_{i,organ} \cdot (K^f_{h,organ}C^f_{h-i,organ} - K^r_{h,organ}C^b_{h-i,organ})$$

$$- V_{i,organ} \cdot (K^f_{ah}C^b_{h-i,organ}C^f_{a-i,organ}$$

$$- K^r_{ah}C^{fb}_{ah-i,organ})$$

$$V_{i,organ}(dC^{ff}_{ah-i,organ}/dt) = J_{ah,organ} - L \cdot C^{ff}_{ah-i,organ}$$

$$+ V_{i,organ}(K^f_{ah}C^f_{a-i,organ}C^f_{h-i,organ}$$

$$- K^r_{ah}C^{ff}_{ah-i,organ}) - V_{i,organ} \cdot (K^f_{ab}(B_{max}$$

$$- C^{fb}_{ab-i,organ} - C^{ffb}_{ahb-i,organ}) \cdot C^{ff}_{ah-i,organ}$$

$$- K^r_{ab}C^{ffb}_{ahb-i,organ})$$

$$- V_{i,organ} \cdot (K^f_{a,organ} \cdot C^{ff}_{ah-i,organ}$$

$$- K^r_{a,organ}C^{bf}_{ah-i,organ})$$

$$- V_{i,organ} \cdot (K^f_{h,organ} \cdot C^{ff}_{ah-i,organ}$$

$$- K^r_{h,organ}C^{fb}_{ah-i,organ})$$

$$V_{i,organ}(dC^{fb}_{ah-i,organ}/dt) = V_{i,organ} \cdot (K^f_{ah}C^f_{a-i,organ}C^b_{h-i,organ}$$

$$- K^r_{ah}C^{fb}_{ah-i,organ})$$

$$+ V_{i,organ} \cdot (K^f_{h,organ} \cdot C^{ff}_{ah-i,organ}$$

$$- K^r_{h,organ}C^{fb}_{ah-i,organ})$$

$$V_{i,organ}(dC^{bf}_{ah-i,organ}/dt) = V_{i,organ} \cdot (K^f_{ah}C^b_{a-i,organ}C^f_{h-i,organ}$$

$$- K^r_{ah}C^{bf}_{ah-i,organ})$$

$$+ V_{i,organ} \cdot (K^f_{a,organ} \cdot C^{ff}_{ah-i,organ}$$

$$- K^r_{a,organ}C^{bf}_{ah-i,organ})$$

$$V_{i,organ}(dC^{ffb}_{ahb-i,organ}/dt) = V_{i,organ}(K^f_{ab}(B_{max} - C^{fb}_{ab-i,organ}$$

$$- C^{ffb}_{ahb-i,organ})C^{ff}_{ah-i,organ} - K^r_{ab}C^{ffb}_{ahb-i,organ})$$

$$+ V_{i,organ} \cdot (K^f_{ah}C^f_{h-i,organ}C^{fb}_{ab-i,organ}$$

$$- K^r_{ah}C^{ffb}_{ahb-i,organ})$$

In each organ, the average concentration of effector agent is:

$$C_{TOT} = (\Sigma_{x=h,ah}C_{x-v}V_v + \Sigma_{x=h,ah}(C^f_{x-i} + C^b_{x-i})V_i + C^{fb}_{ah-i}V_i + C^{bf}_{ah-i}V_i$$

$$+ C^{ffb}_{ahb-i}V_i)/V_{TOT}$$

REFERENCES

1. Goldenberg D, Larson S. Radioimmunodetection in cancer identification. *J Nucl Med* 1992;33:803–814.
2. Goldenberg DM. Introduction to the fifth conference on radioimmunodetection and radioimmunotherapy of cancer. *Cancer Res* 1995;55(suppl):5708s–5709s.
3. Larson SM. Improving the balance between treatment and diagnosis: a role for radioimmunodetection. *Cancer Res* 1995;55(suppl):5756s–5758s.
4. Boucher Y, Baxter LT, Jain RK. Interstitial pressure gradients in tissue-isolated and subcutaneous tumors: implications for therapy. *Cancer Res* 1990;50:4478–4484.
5. Jain RK. Transport of molecules in the tumor interstitium: a review. *Cancer Res* 1987;47:3039–3051.
6. Jain RK. Determinants of tumor blood flow: a review. *Cancer Res* 1988;48:2641–2658.
7. Jain, RK. Barriers to drug delivery in solid tumors. *Sci Am* 1994;271:58–65.
8. Jain, RK. Whitaker Lecture: delivery of molecules, particles, and cells to solid tumors. *Ann Biomed Eng* 1996;24:457–473.
9. Sands H. Radiolabeled monoclonal antibodies for cancer therapy and diagnosis: is it really a chimera? *J Nucl Med* 1992;33:29–32.
10. Goodwin D, Meares C, MaCall M, McTigue M, Chaovapong W. Pretargeting immunoscintigraph of murine tumors with indium-111-labeled bifunctional haptens. *J Nucl Med* 1988;29:226–234.
11. Goodwin D. Tumor pretargeting: almost the bottom line. *J Nucl Med* 1995;36:876–879.
12. Hnatowich DJ, Virzi F, Rusckowski M. Investigations of avidin and biotin for imaging applications. *J Nucl Med* 1987;28:1294–1302.
13. Senter PD, Saulnier MG, Schreiber GJ, et al. Anti-tumor effects of antibody-alkaline phosphatase conjugates in combination with etoposide phosphate. *Proc Natl Acad Sci USA* 1988;85:4842–4846.
14. Senter PD. Enhancement of the in vitro and in vivo antitumor activities of phosphorylated mitomycin C and etoposide derivatives by monoclonal antibody-alkaline phosphatase conjugates. *Cancer Res* 1989;49:5789–5792.
15. Sung C, van Osdol WW, Saga T, Neumann R, Dedrick RL, Weinstein JN. Streptavidin distribution in metastatic tumor pretargeted with a biotinylated monoclonal antibody: theoretical and experimental pharmacokinetics. *Cancer Res* 1994;54:2166–2175.
16. Stickney DR, Slater JB, Kirk GA, Ahlem C, Chang CH, Frincke JM. Bifunctional antibody: ZCE/CHA 111Indium BLEDTA-IV clinical imaging in colorectal carcinoma. *Antibody Immunoconj Radiopharm* 1989;2:1–13.
17. Stickney DR, Anderson LD, Slater JB, et al. Bifunctional antibody: a binary radiopharmaceutical delivery system for imaging colorectal carcinoma. *Cancer Res* 1991;51:6650–6655.
18. van Osdol WW, Sung C, Dedrick R, Weinstein JN. A distributed pharmacokinetic model for two-step imaging and treatment protocols: application to streptavidin-conjugated monoclonal antibodies and radiolabeled biotin. *J Nucl Med* 1993;34:1552–1564.
19. Le Doussal JM, Gruaz-Guyon A, Martin M, Gautherot E, Delaage M, Barbet J. Targeting of indium-111-labeled bivalent hapten to human melanoma mediated by bispecific monoclonal antibody conjugates: imaging of tumors hosted in nude mice. *Cancer Res* 1990;50:3445–3452.
20. Zhu H, Baxter LT, Jain RK. Potential and limitations of radioimmunodetection and radioimmunotherapy with monoclonal antibodies: evaluation using a physiologically based pharmacokinetic model. *J Nucl Med* 1997;731–741.
21. Baxter LT, Zhu H, Mackensen DG, Butler WF, Jain RK. Biodistribution of monoclonal antibodies: scale-up from mouse to man using a physiologically based pharmacokinetic model. *Cancer Res* 1995;55:4611–4622.
22. Baxter LT, Zhu H, Mackensen DG, Jain RK. Physiologically based pharmacokinetic model for specific and nonspecific monoclonal antibodies and fragments in normal tissues and human tumor xenografts in nude mice. *Cancer Res* 1994;54:1517–1528.
23. Watson EE, Stabin G. Siegel JAMIRD formulation. *Med Phys* 1993;20:511–514.
24. Dedrick R. Animal scale-up. *J Pharmacokinet Biopharm* 1973;1:435–461.
25. Fan Y, Baxter LT, Jain RK. Pharmacokinetic analysis of two-step approaches using bifunctional and enzyme-conjugated antibodies. *Cancer Res* 1991;51:3119–3130.
26. Bradwell AR, Fairweather DS, Dykes PW, Keeling A, Vaughan A, Taylor J. Limiting factors in the localization of tumours with radiolabeled antibodies. *Immunol Today* 1985;6:163–170.
27. Bradwell AR, Dykes P, Thomas G. Antibody targeting: theoretical considerations. In: Goldenberg DM, ed. *Cancer imaging with radiolabeled antibodies.* New York: Kluwer Academic Publishers, 1990:11–25.
28. Rockoff SD, Goodenough D, McIntire KR. Theoretical limitations in the immunodiagnostic imaging of cancer with computed tomography and nuclear scanning. *Cancer Res* 1980;40:3054–3058.
29. Yao Z, Zhang M, Kobayashi H, et al. Improved targeting of radiolabeled streptavidin in tumors pretargeted with biotinylated monoclonal antibodies through avidin chase. *J Nucl Med* 1995;36:837–841.
30. Schlom J, Hand PH, Greiner JW, et al. Innovations that influence the pharmacology of monoclonal antibody guided tumor targeting. *Cancer Res* 1990;50(suppl):820s–827s.
31. Buchsbaum DJ. Experimental approaches to increase radiolabeled antibody localization in tumors. *Cancer Res* 1995;55(suppl):5729s–5732s.
32. Knox SJ. Overview of studies on experimental radioimmunotherapy. *Cancer Res* 1995;55(suppl):5832s–5836s.
33. Khaw B, Strauss HW, Narula J. "Magic bullets": from muskets to smart bombs!!! *J Nucl Med* 1993;34:2264–2268.
34. Hellman S. Principles of radiation therapy. In: Rosenberg SA, Hellman S, De Vito V, ed. *Cancer.* Philadelphia: J. B. Lippincott, 1992:2490.
35. Yuan F, Baxter LT, Jain RK. Pharmacokinetic analysis of two-step approaches using bifunctional and enzyme-conjugated antibodies. *Cancer Res* 1991;51:3119–3130.
36. Sung C, van Osdol W. Pharamcokinetic comparison of direct antibody targeting with pretargeting protocols based on streptavidin–biotin binding. *J Nucl Med* 1995;36:867–876.
37. Hindmarsh AC. LSODE and LSODI, two new initial value ordinary differential equation solvers. *ACM Signum Newsletter* 1980;15:10–11.
38. Rippe B, Haraldsson B. Fluid and protein fluxes across small and large pores in the microvasculature. Application of two-pore equations. *Acta Physiol Scand* 1987;131:411–428.
39. Rippe B, Haraldsson B. Transport of macromolecules across microvascular walls: the two-pore theory. *Physiol Rev* 1994;74:163–219.